Biogeosciences Discuss., 11, 10737–10777, 2014
www.biogeosciences-discuss.net/11/10737/2014/
doi:10.5194/bgd-11-10737-2014

Biogeosciences Discussions
Open Access

Influence of meteorology and anthropogenic pollution on chemical flux divergence of the NO-NO_2-O_3 triad above and within a natural grassland canopy

D. Plake[1], M. Sörgel[1], P. Stella[1,*], A. Held[2], and I. Trebs[1,]**

[1]Max Planck Institute for Chemistry, Biogeochemistry Department, P. O. Box 3060, 55020 Mainz, Germany
[2]University of Bayreuth, Junior Professorship in Atmospheric Chemistry, Bayreuth, Germany
[*]now at: AgroParisTech, UMR INRA/AgroParisTech SAD-APT, Paris, France
[**]now at: Centre de Recherche Public – Gabriel Lippmann, Department Environment and Agro-biotechnologies, 41 rue du Brill, 4422 Belvaux, Luxembourg

Received: 9 May 2014 – Accepted: 21 June 2014 – Published: 14 July 2014

Correspondence to: D. Plake (daniel.plake@mpic.de)

Published by Copernicus Publications on behalf of the European Geosciences Union.

Abstract

The detailed understanding of surface–atmosphere exchange of reactive trace gas species is a crucial precondition for reliable modeling of processes in atmospheric chemistry. Plant canopies significantly impact the atmospheric budget of trace gases. In the past, many studies focused on taller forest canopies or crops, where the bulk plant material is concentrated in the uppermost canopy layer. However, within grasslands, a land-cover class that globally covers vast terrestrial areas, the canopy structure is fundamentally different, as the main biomass is concentrated in the lowest canopy part. This has obvious implications for aerodynamic in-canopy transport, and consequently also impacts on global budgets of key species in atmospheric chemistry such as nitric oxide (NO), nitrogen dioxide (NO_2) and ozone (O_3).

This study presents for the first time a comprehensive data set of directly measured in-canopy transport times and aerodynamic resistances, chemical timescales, Damköhler numbers, trace gas and micrometeorological measurements for a natural grassland canopy (canopy height = 0.6 m). Special attention is paid to the impact of contrasting meteorological and air chemical conditions on in-canopy transport and chemical flux divergence. Our results show that the grassland canopy is decoupled throughout the day. In the lower canopy, the measured transport times are fastest during nighttime, which is due to convection during nighttime and stable stratification during daytime in this layer. The inverse was found in the layers above. During periods of low wind speed and high NO_x ($NO + NO_2$) levels, the effect of canopy decoupling on trace gas transport was found especially distinct. The aerodynamic resistance in the lower canopy (0.04–0.2 m) was around 1000 s m^{-1}, thus as high as values from literature representing the lowest meter of an Amazonian rain forest canopy. The aerodynamic resistance representing the bulk canopy was found to be more than 3–4 times higher as in forests. Calculated Damköhler numbers (ratio of transport and chemical timescales) suggested a strong flux divergence for the NO-NO_2-O_3 triad within the canopy during daytime. At that time, the timescale of NO_2 plant uptake ranged from

BGD
11, 10737–10777, 2014

90 to 160 s and was the fastest relevant timescale, i.e. faster than the reaction of NO and O_3. Thus, our results clearly reveal that grassland canopies of similar structure have a strong potential to retain soil emitted NO by uptake of NO_2 by the plants. Furthermore, a photo-chemical O_3 production above the canopy was observed, which resulted from a surplus of NO_2 from the NO-NO_2-O_3 photostationary state. The O_3 production was one order of magnitude higher during high NO_x than during low NO_x periods and resulted in an O_3 flux underestimation, which was observed for the first time.

1 Introduction

Nitric oxide (NO) and nitrogen dioxide (NO_2) play a crucial role in air chemistry since they act as key catalysts for ozone (O_3) production and are therefore involved in the generation of hydroxyl radicals (OH) (Crutzen, 1973). The most significant tropospheric source of O_3 is initiated by photochemical dissociation of NO_2 and subsequent reaction of the oxygen (O) atom with molecular oxygen:

$$NO_2 + h\nu(\lambda < 420\,\text{nm}) \rightarrow NO + O(^3P) \quad \text{(R1)}$$

$$O(^3P) + O_2 + M \rightarrow O_3 + M \quad \text{(R2)}$$

When O_3 is present, it may oxidize NO and re-form NO_2:

$$O_3 + NO \xrightarrow{k_3} NO_2 + O_2 \quad \text{(R3)}$$

In the absence of additional reactions, Reactions (R1)–(R3) represent a null cycle. Beside Reactions (R1)–(R3), NO is oxidized by peroxy radicals constituting an additional important net O_3 production pathway in the troposphere (Warneck, 2000).

Dry deposition to terrestrial surfaces, especially to plant canopies, is an important sink for tropospheric O_3 and NO_2. The uncertainties of dry deposition estimates are substantially higher for NO_2, because its net ecosystem exchange can be bi-directional

BGD
11, 10737–10777, 2014

depending on the ambient NO_2 levels (Lerdau et al., 2000). O_3 instead is exclusively deposited to surfaces. In contrast, NO is known to be mainly net emitted from nearly all soil types. Biogenic NO soil emissions contribute about 20 % to the global NO_x ($NO + NO_2$) emissions (IPPC, 2007), highlighting the need of careful investigations on NO soil–atmosphere exchange.

A major challenge for studies investigating surface–atmosphere exchange fluxes of these reactive trace gases is the presence of plant canopies. These significantly modify the turbulent properties of the surface and thus alter trace gas exchange. Most previous studies focused on taller canopies such as forests. However, grassland canopies represent a highly important land cover class covering globally 41 % and Europe-wide 19 % of the terrestrial land surface (Suttie et al., 2005; Kasanko et al., 2011). In contrast to forests, grasslands feature the main bulk plant area density near the soil (e.g., Ripley and Redman, 1976; Jäggi et al., 2006), accompanied with mean distances between plant elements of only some millimeters (Aylor et al., 1993). Organized coherent structures govern turbulence dynamics within and above plant canopies (Finnigan, 2000). The mean in-canopy transport is slower than above the canopy (e.g., Nemitz et al., 2009). This modification of in-canopy transport has important implications for global atmospheric chemistry. Plant canopies and the soil below are biologically actively emitting and taking up reactive trace gases, and they may provide sufficient time for fast chemical reactions to occur within the canopy (Nemitz et al., 2009). Subsequently they modify surface exchange fluxes (e.g., Rinne et al., 2012). For instance, ammonia can be released by a part of the canopy and taken up by another (Nemitz et al., 2000; Denmead et al., 2007). In addition, recapturing of NO_2 originating from biogenic soil NO emissions after reaction with O_3 within plant canopies (Rummel et al., 2002) is accounted for in global models by a so-called canopy reduction factor for NO_x (Yienger and Levy, 1995). However, these estimates are based on only one single experiment in an Amazon rain forest (Bakwin et al., 1990), and a subsequent model analysis (Jacob and Wofsy, 1990). Canopy reduction for grasslands and other ecosystems was not experimentally studied up to now. Consequently, the contrasting canopy structure

BGD
11, 10737–10777, 2014

of grassland and forest ecosystems highlights the need for a detailed analysis and an evaluation of the NO_x canopy reduction factor of 64 % suggested by Yienger and Levy (1995) for temperate grassland.

Net ecosystem exchange fluxes are typically measured at a certain height above the canopy. They rely on the constant flux assumption (e.g., Swinbank, 1968), which however, may be violated for reactive trace gases within or just above the vegetation. To assess the potential chemical divergence of exchange fluxes, the Damköhler number (DA) has commonly been applied (e.g., Rinne et al., 2012). DA is calculated as the ratio of the transport time (τ_{tr}) and the characteristic chemical timescale (τ_{ch}):

$$DA = \frac{\tau_{tr}}{\tau_{ch}} \quad (1)$$

Hence, DA above unity indicates that chemical reactions occur significantly faster than the transport (flux divergence), whereas DA smaller than 0.1 indicate the reverse case. The range in-between is commonly addressed as a critical range, where an impact of chemistry cannot be excluded (Stella et al., 2013).

In this paper, we present directly measured transport times, chemical timescales and corresponding Damköhler numbers for three layers above and within a natural grassland canopy under contrasting meteorological and air chemical conditions. For the first time, such a comprehensive analysis involving trace gas and micrometeorological measurements is made for a grassland canopy. Furthermore, the consequences of in-canopy processes for NO_x canopy reduction and simultaneously measured O_3 deposition fluxes will be discussed.

2 Material and methods

2.1 Site description

We performed an intensive field experiment from July to September 2011 at the estate of the Mainz-Finthen Airport in Rhineland-Palatinate, Germany (further details given

BGD
11, 10737–10777, 2014

in Plake and Trebs, 2013; Plake et al., 2014; Moravek et al., 2014). The vegetation at the site was nutrient-poor grassland with a mean canopy height (h_c) of 0.6 m and a leaf area index (LAI) of 4.8 m^2 m^{-2}. A list of species and an LAI profile are given in Plake et al. (2014), with the latter indicating a high biomass density below 0.2 m corresponding to 85 % of the total LAI. Topographically located on a plateau 150 m above the Rhine valley, the site was situated about 9 km south-west of the city center of Mainz. The site was surrounded by villages and motorways in a distance of 2 to 6 km and 4 to 15 km, respectively. The surrounding area was mainly characterized by agricultural use for vineyards, orchards and crops. The fetch was largest in south-western direction without significant anthropogenic pollution sources.

2.2 Experimental setup

A vertical Thoron (Tn) profile system was operated at $z_1 = 0.04$ m, $z_2 = 0.2$ m and $z_3 = 0.8$ m for the direct determination of transport times (for details see Plake and Trebs, 2013). Vertical profiles of NO, NO_2, O_3 and CO_2 were measured at z_1, z_2, z_3 and additionally at $z_4 = 4.0$ m by a system described in detail by Plake et al. (2014). This study is based on simultaneous operation of both vertical profile systems at identical heights and, thus is focused on the period from 19 August to 26 September 2011 were both systems were operational. Vertical profiles of temperature (HMT337, Vaisala, Helsinki, Finland), wind speed and direction (WS425, Vaisala, Helsinki, Finland) were installed at 0.2 m, 0.8 m, 1.5 m, 2.5 m, 4.0 m. Soil temperature (107L, Campbell Scientific Inc., Logan, USA) was measured at −0.02 m. Global radiation (G) and the NO_2 photolysis frequency (j_{NO_2}) were measured at a height of 2.5 m with a net radiometer (CNR1, Kipp&Zonen, Delft, Netherlands), and a filter radiometer (Meteorology Consult GmbH, Glashütten, Germany), respectively. The data of temperature, wind and radiation were recorded by a data logger (CR3000, Campbell Scientific) every 10 s. A three dimensional sonic anemometer (CSAT-3, Campbell Scientific) placed at $z_{ref} = 3.0$ m measured 3-D wind and temperature at 20 Hz and the data were recorded by a CR3000 data logger. The friction velocity (u_*) and stability functions (z/L) were computed using

BGD
11, 10737–10777, 2014

the TK3 software (see Mauder and Foken, 2011). Eddy covariance fluxes of O_3 were simultaneously measured and are described in detail by Plake et al. (2014).

2.3 Theory

The data analysis was carried out for three individual layers (L_{1-3}), which were named in ascending order starting at the soil surface. Hence, L_1 was the lower canopy layer between the corresponding measurement heights z_{1-2} ($\Delta z(L_1) = 0.16$ m), L_2 the upper canopy layer between z_{2-3} ($\Delta z(L_2) = 0.6$ m), and L_3 the layer above the canopy between z_3 and z_{ref} ($\Delta z(L_3) = 2.2$ m). As shown in Plake et al. (2014) the vertical trace gas gradients between z_{ref} and z_4 were negligible, allowing the use of mixing ratios measured at z_4 for L_3.

2.3.1 Chemical timescales

The overall chemical timescale τ_{ch} (in s) of the NO-NO_2-O_3 triad (Lenschow, 1982) was calculated for each layer (L_i, $i = 1,2,3$) as:

$$\tau_{\mathrm{ch}}(L_i) = \frac{2}{\sqrt{\begin{array}{l} j_{\mathrm{NO_2}}(L_i) \times k_3(L_i) \times (N_{\mathrm{O_3}}(L_i) + N_{\mathrm{NO}}(L_i))^2 + 2 j_{\mathrm{NO_2}}(L_i) \\ \times k_3(L_i) \times (N_{\mathrm{O_3}}(L_i) + N_{\mathrm{NO}}(L_i) + 2N_{\mathrm{NO_2}}(L_i))^2 \end{array}}} \quad (2)$$

where $N_{\mathrm{O_3}}$, N_{NO} and $N_{\mathrm{NO_2}}$ are the number densities (in molecules cm^{-3}) of O_3, NO and NO_2 for L_{1-3}, and k_3 the reaction rate constant of Reaction (R3) (in cm^3 molecule^{-1} s^{-1}) according to Atkinson et al. (2004). Geometric means of the number densities at z_{1-4} were used in Eq. (2) to account for non-linear profiles (e.g., $N_{\mathrm{NO}}(L_1) = \sqrt{N_{\mathrm{NO}}(z_1) \times N_{\mathrm{NO}}(z_2)}$).

BGD
11, 10737–10777, 2014

2.3.2 NO_2 photolysis within the canopy

The data gaps in the measured time series of j_{NO_2} (in s^{-1}) above the canopy were filled using the parameterization of j_{NO_2} as a function of G (in $W\,m^{-2}$) by Trebs et al. (2009). This approach was also used to parameterize in-canopy j_{NO_2} from a vertical in-canopy profile of G. The latter was calculated as function of the LAI profile using the method of Monsi and Saeki (1953):

$$G(\mathrm{LAI}) = G_0 \times \exp^{(-k_{ex} \times \mathrm{LAI})} \quad (3)$$

where G_0 (in $W\,m^{-2}$) is the above-canopy G and k_{ex} is the dimensionless extinction coefficient of the canopy. In this study, the extinction coefficient of barley ($k_{ex} = 0.69$ by Monteith and Unsworth, 1990) was used. First G(LAI) was deduced and then converted into j_{NO_2}. Finally, geometric means of j_{NO_2} were calculated for $j_{NO_2}(L_{1-3})$.

2.3.3 Transport times

For L_3, height integrated transport times $\tau_{tr}(L_3)$ (in s) were derived by multiplying the aerodynamic resistance ($R_a(L_3)$) (e.g., Hicks et al., 1987; Erisman et al., 1994) with the layer thickness ($\Delta z(L_3)$) (cf. Stella et al., 2013):

$$\tau_{tr}(L_3) = R_a(L_3) \times \Delta z(L_3) \quad (4)$$

$$R_a(L_3) = \frac{1}{\kappa \times u_*}\left[\ln\left(\frac{z_{ref} - d}{z_3 - d}\right) - \Psi_H\left(\frac{z_{ref} - d}{L}\right) + \Psi_H\left(\frac{z_3 - d}{L}\right)\right] \quad (5)$$

where κ was the von-Kàrmàn constant (= 0.4), d the displacement height ($d = 0.75 \times h_c$), Ψ_H the stability correction function for heat (Foken, 2008) and L the Obukhov length.

BGD
11, 10737–10777, 2014

In the canopy, $\tau_{tr}(L_i, i = 1,2)$ were derived from the vertical Tn profiles (Lehmann et al., 1999; Plake and Trebs, 2013):

$$\tau_{tr}(L_i) = \ln\left[\frac{C_{Tn_{z_l}}(L_i)}{C_{Tn_{z_u}}(L_i)}\right]/\lambda \quad (6)$$

where $C_{Tn_{z_l}}$ and $C_{Tn_{z_u}}$ were the measured Tn concentrations (in Bq m^{-3}) at the lower (z_l) and upper (z_u) heights of L_i, and λ the radioactive decay rate $\lambda = \ln 2/T_{0.5} = 0.0125\,s^{-1}$ (Hänsel and Neumann, 1995).

3 Results

3.1 Meteorological conditions and mixing ratios

Figure 1a displays the dominance of south westerly winds at the site during 45 % of the field experiment and their relation to relatively low NO_x levels (< 3 ppb). Contrastingly, winds from the north eastern sector were characterized by high NO_x levels often above 13 ppb (Fig. 1a). High NO_x episodes (up to 40 ppb) were accompanied with low wind speed (< 3 m s^{-1}) and low NO_x (< 5 ppb) with wind speed greater 3 m s^{-1} as shown in Fig. 1b. The measured CO_2 levels generally showed a similar pattern, while O_3 levels exhibited the opposite dependency on ws.

For further data analysis, defined criteria allowed to account for these specific relationships. In order to clearly separate entire days (24 h) of contrasting conditions from each other, the criteria were defined as low NO_x or high NO_x periods when (i) the mean daytime ws was > 3 m s^{-1} and the wind direction mainly ranged between 180 and 270°, or (ii) the mean daytime ws was < 3 m s^{-1} and the wind direction was mainly outside 180–270°, respectively. The wind direction definition was fulfilled during 96 % of the low NO_x periods and during 84 % of the high NO_x periods. Following these criteria, we

BGD
11, 10737–10777, 2014

identified eleven and nine days as low and high NO_x periods, respectively, which were separately analyzed.

3.2 Vertical profiles of trace gases

Since the wind field is the driver of vertical exchange of scalars such as trace gases between vegetation and the atmosphere (Finnigan, 2000), it affects their vertical distribution. Passive tracers such as Rn and CO_2 are used especially at nighttime as indicators for vertical exchange processes within plant canopies (e.g., Trumbore et al., 1990; Nemitz et al., 2009). Generally, nighttime ws values of the low and high NO_x periods were accordingly higher and lower, respectively. This was reflected by the in-canopy concentrations of both Rn and CO_2 (Fig. 2a–d). During nighttime when both gases are exclusively emitted by soil, a rather weak enrichment within the canopy (Fig. 2a and c) reflected higher ws and thus enhanced exchange during the low NO_x periods. In comparison, during the high NO_x periods a strong in-canopy CO_2 and Rn accumulation was observed (Fig. 2b and d). During daytime photosynthesis prohibits the use of CO_2 as passive tracer, whereas Rn profiles are still useful as no biological processes such as stomatal uptake affect its concentration (Lehmann et al., 1999). The vertical exchange is generally enhanced during daytime causing dilution of the in-canopy Rn concentrations, which was especially pronounced in the low NO_x periods (Fig. 2a) and was less evident during the high NO_x periods (Fig. 2b), due to generally lower wind speed during the latter periods.

The vertical distribution of O_3 (Fig. 2e and f) reflected a typical pattern with lower mixing ratios closer to the ground and higher mixing ratios above. The diurnal O_3 maximum occurred during the afternoon around 16:00 CET (= UTC +1). Nevertheless, in the low NO_x periods the diurnal O_3 maximum was much less pronounced compared to the high NO_x periods with 35 ppb and 50 ppb, respectively. Furthermore, characteristic vertical O_3 distributions were observed during the low and high NO_x periods. Nighttime O_3 gradients were less pronounced during the low NO_x than during the high NO_x periods. Median in-canopy values of O_3 were 10–20 ppb and 20–25 ppb above-

BGD
11, 10737–10777, 2014

canopy during the low NO_x periods (Fig. 2e). During the high NO_x periods 1–6 ppb were measured in the canopy and above-canopy 10–25 ppb (Fig. 2f).

During both the low and the high NO_x periods, significantly enhanced NO mixing ratios prevailed during the morning hours from 06:00 to 14:00 CET (Fig. 2g and h) with median diurnal maxima of 0.6 ppb and 7.2 ppb, respectively, both occurring at 10:00 CET (not visible in Fig. 2h due to scaling). The NO mixing ratios decreased afterwards to approach nighttime minima. These were characterized by small vertical NO gradients during both periods. During low NO_x nights, NO appeared to be mainly present in the in-canopy air layer, with median mixing ratios at z_1 and z_2 of ≤ 0.1 ppb. The median values at z_1 and z_2 during the high NO_x periods were ≤ 0.3 ppb, respectively.

NO_2 mixing ratios were generally found to increase with height (Fig. 2i and j), featuring significantly stronger vertical differences during the high NO_x periods. Similar to NO, also NO_2 mixing ratios were enhanced throughout the profile during the morning hours of both, low and high NO_x periods, with corresponding values of 1–2.5 ppb and 6–14 ppb, respectively. At nighttime, comparable NO_2 mixing ratios of around 1 ppb prevailed during both periods at z_1. NO_2 showed stronger gradients above the canopy during the high NO_x periods. The diurnal NO_2 minima during low and high NO_x periods were observed between 12–16 CET and 14–16 CET, respectively.

3.3 Vertical profiles of chemical timescales

The obtained values for τ_{ch} were generally higher during nighttime than during daytime (Fig. 3a, d and g) and decrease from L_3 to L_1. The validity of our applied criteria for separation between low and high NO_x periods, is shown by the median values (brown and green lines) nearly adjoined the interquartile range of the overall data set. Significantly higher τ_{ch} values prevailed during nighttime of the high NO_x periods, ranging from 300 to 2500 s in L_{1-3}. In contrast, low NO_x periods were characterized by τ_{ch} of 250–800 s in L_{1-3}. However, during daytime τ_{ch} was within 100–200 s in L_{1-3} for both

BGD
11, 10737–10777, 2014

periods. During the low NO_x periods τ_{ch} values were slightly higher compared to the high NO_x periods.

3.4 Vertical profiles of transport times

The median $\tau_{tr}(L_3)$ of all data Fig. 3b was one order of magnitude smaller during noon than at midnight with 30 and 200 s, respectively. As for τ_{ch} (Sect. 3.3), also in the case of τ_{tr} the medians of the low and high NO_x periods adjoined the interquartile range of the overall data set. For example, $\tau_{tr}(L_3)$ in the low NO_x periods never exceeded $\tau_{tr}(L_3)$ in the high NO_x periods (cf. Fig. 3b). The difference of $\tau_{tr}(L_3)$ between noon and midnight was largest in the high NO_x and smallest during the low NO_x periods with 470 and 40 s, respectively. Compared to L_{1-2} (Fig. 3e and h), the extreme values of the entire τ_{tr} data set were found above the canopy in L_3. The overall τ_{tr} minimum occurred during daytime of the low NO_x periods, and the maximum during nighttime of the high NO_x periods in L_3.

The diurnal course of $\tau_{tr}(L_2)$ from the entire data set in Fig. 3e exhibited a similar pattern as $\tau_{tr}(L_3)$, with higher $\tau_{tr}(L_2)$ during nighttime than during daytime. Representative nighttime and daytime values were 200 and 100 s, respectively, and a similar nighttime separation between the low and high NO_x periods as in Fig. 3b was observed.

In contrast, both diurnal $\tau_{tr}(L_1)$ medians representing all data and the high NO_x periods (Fig. 3 h) were slightly higher during daytime between 08:00 and 13:00 CET than at nighttime with around 200 and 75–175 s, respectively. In the low NO_x periods, the median $\tau_{tr}(L_1)$ was relatively constant throughout the day with about 200 s. The pattern of $\tau_{tr}(L_1)$ was generally opposite to L_{2-3}, with faster $\tau_{tr}(L_1)$ in the high NO_x periods than in the low NO_x periods.

3.5 Vertical profiles of Damköhler numbers

The values for $DA(L_3)$ presented in Fig. 3c were generally smaller during daytime than during nighttime. They exhibited a diurnal minimum of 0.2 and a maximum of 1.3 at

BGD
11, 10737–10777, 2014

08:00 and 21:00 CET, respectively. In the low NO_x periods, the difference of the $DA(L_3)$ median ($0.2 < DA(L_3) < 0.3$), to a DA of unity was highest whereas in the high NO_x periods $DA(L_3)$ remained at higher median values ($0.3 < DA(L_3) < 3.9$).

In contrast, the diurnal course of $DA(L_2)$ in Fig. 3f exhibited its maximum of 1.25 at 15:00 CET and nighttime minima of about 0.3. The difference in $DA(L_2)$ between the low and high NO_x periods was not as pronounced as for $DA(L_3)$. It became most obvious from 15:00 to 24:00 CET with lower $DA(L_2)$ in the low NO_x periods. Hence, both $DA(L_{2,3})$ values throughout the day were within the critical range for DA or above under all conditions.

Interestingly, the diurnal course of $DA(L_1)$ (Fig. 3i) appeared mirror-inverted to $DA(L_3)$, with highest and lowest DA during daytime and nighttime, respectively. The diurnal median of $DA(L_1)$ partly exhibited values below 0.1 (transport dominates) during nighttime of the high NO_x periods, values above unity (chemistry dominates) from 12:00 to 17:00 CET under all conditions, and between 0.1 and unity during nighttime in the overall data set and in the low NO_x periods.

4 Discussion

4.1 Transport times and resistances

4.1.1 Thermal stratification

The diurnal courses of the temperature differences $\Delta T(L_{1-3})$ in Fig. 4a–c describe the stability in each layer. They clearly indicated contrasting stability conditions in L_1 and L_{2-3}. During daytime, negative values of $\Delta T(L_{2-3})$ reflected unstable conditions, while positive $\Delta T(L_1)$ reflected stable conditions. In contrast, at nighttime these conditions were reversed. Similar diurnal cycles of stratifications are observed for other canopies (cf. Jacobs et al., 1994; Kruijt et al., 2000; Nemitz et al., 2000), and are known to decouple the lower canopy from the air layers above (cf. Fig. 4d). Canopy coupling regimes

BGD
11, 10737–10777, 2014

are typically classified according to the detection of coherent structures in high frequency time series of scalars such as temperature (e.g. Foken et al., 2012; Dupont and Patton, 2012). In our data set $\Delta T(L_1)$ could be used to explain why $\tau_{tr}(L_1)$ was generally smaller, i.e. transport was faster, during night than daytime (Fig. 3 h). The soil released stored heat as thermal plumes during nighttime that drove an in-canopy nighttime convection which reached up to the height of the temperature inversion as explained by Dupont and Patton (2012) or Jacobs et al. (1994). This effect caused the lower $\tau_{tr}(L_1)$ during nighttime. The $\tau_{tr}(L_1)$ maximum of 200 s from 08:00 to 13:00 CET could accordingly been attributed to positive $\Delta T(L_1)$ values at that time indicating a stable stratification. In all layers the thermal stratification was stronger during the high NO_x periods and weaker during the low NO_x periods (Fig. 4a–c). This was caused by higher wind speed during the low NO_x periods that yielded better mixing and thus the vertical temperature differences were smaller.

4.1.2 Aerodynamic resistances and transport times

Aerodynamic resistances (R_a) are important input parameters for modeling studies on surface–atmosphere exchange fluxes. They represent transport times through a layer, normalized by the layer thickness ($R_a = \tau_{tr}/\Delta z$). In cases when the thicknesses of two layers under consideration differ, the effectiveness of transport can be represented by the corresponding aerodynamic resistances. On the other hand, transport times are required to evaluate the influence of chemical reactions on fluxes (e.g., DA).

Aerodynamic in-canopy resistances (R_{ac}) are typically parameterized as function of u^* and LAI (e.g., van Pul and Jacobs, 1994; Personne et al., 2009). These parameterizations are based on experiments above e.g., crops such as maize (van Pul and Jacobs, 1994) and consider a homogeneous vertically leaf distribution (Personne et al., 2009). However, this approximation may differ substantially within grassland canopies, as their structure is characterized by high biomass density in the lowest layer (cf. Sect. 2.1).

BGD
11, 10737–10777, 2014

The usefulness of our results is underlined by the direct assessment of measured R_{ac} values. From Eq. (6) we can assess R_{ac} for different canopy layers (L_1, L_2 and for the whole canopy ($\tau_{tr}(z_1, z_3)$; $\Delta z = z_3 - z_1$)) within the grassland canopy (cf. Fig. 5). In the lower canopy, $R_{ac}(L_1)$ was generally highest with medians of 900 to 1000 s m^{-1} during nighttime and 1000 to 1300 s m^{-1} during daytime (Fig. 5). In comparison, Gut et al. (2002) found the aerodynamic resistance in the lowest meter of an Amazonian rain forest canopy in a similar range and showing the same diurnal pattern with 600 s m^{-1} during nighttime and 1700 s m^{-1} during daytime.

As found for the transport times, the diurnal course of R_{ac} was inversed in the layers above (Fig. 5). In the upper canopy, the median of $R_{ac}(L_2)$ typically ranged around 300 s m^{-1} during nighttime and around 150 s m^{-1} during daytime. In comparison, above the canopy the median of $R_a(L_3)$ (Eq. 5) was substantially lower with around 80 and 15 s m^{-1} during nighttime and daytime, respectively. Consequently, the aerodynamic resistances in and above the canopy ($R_{ac}(L_{1,2})$ and $R_a(L_3)$) differed by almost two orders of magnitude during daytime, and by one order of magnitude during nighttime. Accordingly, the efficiency of aerodynamic transport decreased with height, even if the transport times were partly shorter in L_1 compared to L_3. The R_{ac} for the whole canopy (Fig. 5) ranged in-between $R_{ac}(L_1)$ and $R_{ac}(L_2)$ with 440 s m^{-1} during nighttime and 360 s m^{-1} during daytime. The opposite diurnal courses of both, $R_{ac}(L_1)$ and $R_{ac}(L_2)$ have an impact on R_{ac}, which in turn showed a smaller diurnal variation. As L_2 contained around 80 % of the layer thickness between z_1 and z_3 (cf. Fig. 5), R_{ac} was closer to $R_{ac}(L_2)$.

The median transport time through the 0.6 m high natural grassland canopy (also referred to as "canopy flushing time") was presented in the related study of Plake and Trebs (2013) for the same experiment. It was measured using the vertical thoron profile between z_1 and z_3 (Eq. 6). The canopy flushing time is consistent with the sum of $\tau_{tr}(L_1)$ and $\tau_{tr}(L_2)$ in this manuscript (cf. Fig. 7 below) and represents the in-canopy layer down to $0.07 \times h_c$ (z_1/h_c). It was determined to be ≤ 6 min exhibiting only small daytime/nighttime variation. Simon et al. (2005) reported canopy flushing times based

BGD
11, 10737–10777, 2014

on radon measurements within a 40 m high rain forest canopy. For the layer between h_c and $0.13 \times h_c$ (canopy top to trunk space), they determined flushing times of around 60 min during any time of the day. As in the grassland canopy in Mainz-Finthen, nighttime in-canopy convection accounted for the small daytime/nighttime variation in their study. Normalization of their canopy flushing time by the layer thickness yielded R_{ac} in the order of $100\,s\,m^{-1}$, which is around 3–4 times lower than the corresponding R_{ac} of the grassland site. Other studies (Holzinger et al., 2005; Rummel, 2005) based on surface renewal models reported somewhat lower flushing times. Rummel (2005) found flushing times in a 32 m high rain forest canopy of ≤ 200 s during daytime, which correspond to R_{ac} values $\leq 10\,s\,m^{-1}$. In the same way Holzinger et al. (2005) determined flushing times of 90 s during daytime and around 300 s during nighttime within a 6 m high scrubby pine forest. Corresponding R_{ac} values were in the order of 20 and $60\,s\,m^{-1}$, respectively.

Thus, it is important to note that even if the canopy height of natural grassland canopies is small compared to forests (around 1–10 %); the corresponding canopy flushing times are of the same order of magnitude as those reported for forest canopies (10–400 %). The typically high biomass density in the lower canopy of grasslands (e.g., Jäggi et al., 2006; Nemitz et al., 2009) is the most obvious explanation. It provides a large aerodynamic resistance ($> 900\,s\,m^{-1}$) in a small layer adjacent to the ground (here: $R_{ac}(L_1)$). The aerodynamic resistance is large enough to increase the overall aerodynamic resistance of the whole canopy (R_{ac}) by 50 % and 140 % during night and daytime, respectively. Consequently, R_{ac} of the grassland canopy was found at least 3–4 times higher than R_{ac} values representing corresponding in-canopy layers of forests taken from literature.

Plake and Trebs (2013) compared their directly measured transport times with the parameterizations of van Pul and Jacobs (1994) and Personne et al. (2009). They found that none of the parameterizations was able to reproduce the entire diurnal course of the in-canopy transport. An agreement with the measured transport times was either

BGD
11, 10737–10777, 2014

found during daytime (Personne et al., 2009) or nighttime (van Pul and Jacobs, 1994), underlining the need for more direct measurements on in-canopy transport.

4.2 Chemical timescales

The non-linear profiles of NO, NO_2 and O_3 might have introduced uncertainties in $\tau_{ch}(L_{1-3})$. The potential uncertainties due to averaging were investigated by determining the individual $\tau_{ch}(z_{1-4})$ and their subsequent comparison with $\tau_{ch}(L_{1-3})$. In L_1, L_2 and L_3 they were found to be $\leq 13\,\%$, $\leq 4\,\%$ and $\leq 2\,\%$, respectively, during daytime under any condition. During nighttime, the uncertainties in L_2 and L_3 were found to be 6 and 2 % during the low NO_x periods and 57 % and 13 % during the high NO_x periods, respectively. In L_1 the uncertainty during nighttime was 30 % for all conditions. Furthermore, the in-canopy parameterization of j_{NO_2} might have introduced additional uncertainties since (i) in reality the attenuation of in-canopy radiation might be more complex than described in Eq. (3), and (ii) the parameterization of j_{NO_2} from G is prone to uncertainties of $> 40\,\%$ for $G < 100\,W\,m^{-2}$, 10–40 % for $G = 100$–$500\,W\,m^{-2}$ and $\leq 10\,\%$ for $G > 500\,W\,m^{-2}$ (Trebs et al., 2009).

The diurnal maxima and minima of $\tau_{ch}(L_{1-3})$ (Fig. 3a, d and g) were found to coincide with the O_3 minima and maxima (Fig. 2e and f), respectively. The impact of the terms in Eq. (2) on $\tau_{ch}(L_3)$ was examined by a correlation coefficient analysis. It was found to be highest for O_3 followed by NO_2 and NO with $r = -0.57$, $r = 0.46$ and $r = -0.07$, respectively. As the average air-chemical situation in Mainz-Finthen, was characterized by a surplus of O_3 compared to NO_2 or NO (cf. Sect. 3.2), the magnitude of $\tau_{ch}(L_3)$ was most affected by the mixing ratios of O_3. In contrast, NO was generally less abundant, which explained the low overall impact on $\tau_{ch}(L_3)$. Only under high NO_x situations, when NO levels were above 5 ppb (cf. Sect. 3.1), an increased impact of NO on $\tau_{ch}(L_3)$ was found.

Figure 6a summarizes the chemical timescales. The temporal variation in τ_{ch}, expressed by higher nighttime and lower daytime values, can be considered as a rather

BGD
11, 10737–10777, 2014

typical pattern based on the diurnal courses of NO, NO_2 and O_3 (Fig. 2e–j) and their strong photochemical link. The vertical variation in $\tau_{ch}(L_{1-3})$ was on the one hand caused by the attenuation of j_{NO_2} in the canopy, and on the other hand by generally increasing mixing ratios of NO, NO_2 and O_3 with height (Fig. 2e–j). It should be noted, that the latter was a site characteristic issue. Insignificant NO soil emissions were measured by Plake et al. (2014), and were underlined by weak in-canopy NO gradients (Fig. 2g and h). As already discussed in the previous paragraph, generally low NO, NO_2 and O_3 mixing ratios tend to cause high τ_{ch} values and vice versa. Consequently, at a site with higher NO emissions as e.g., an intensively managed agricultural field, the vertical τ_{ch} profile would most likely feature smaller vertical differences.

The extremely high $\tau_{ch}(L_{1,})$ during nighttime of the high NO_x periods (Fig. 6a) were a direct consequence of canopy decoupling (cf. Sect. 4.1.1). Transport of O_3 and NO_2 into the lower canopy was suppressed by the temperature inversion (cf. Fig. 2f and j). The residual O_3 and NO_2 molecules were convectively circulated within the lower canopy and, subsequently deposited efficiently to surfaces until both almost disappeared in the early morning (Fig. 2f and j). Thus, the negligible NO emissions together with the suppressed supply of O_3 and NO_2 from above, yielded simultaneously very low mixing ratios of all three species, that in turn led to the extremely high $\tau_{ch}(L_{1,})$ values.

Our results are in line with those of Stella et al. (2013) who reported median diurnal τ_{ch} of 80–300 s and 150–600 s above and within the canopy, respectively, for an intensively managed meadow. Their in-canopy τ_{ch} maximum was somewhat lower than in Mainz-Finthen, which might be attributed to NO soil emissions or to averaging of different layers.

Since Eq. (2) exclusively considers Reactions (R1) and (R3), additional reactions may have biased the obtained τ_{ch} values to a certain extent. For instance, the oxidation of NO to NO_2 by peroxy radicals (Sect. 1), or reactions between volatile organic compounds (VOCs) and O_3 (e.g., Atkinson and Arey, 2003) might have influenced ambient NO, NO_2 and O_3 levels. Simultaneously measured VOC mixing ratios featured very small values at our site (e.g., isoprene < 0.7 ppb, monoterpene < 0.3 ppb,

BGD
11, 10737–10777, 2014

J. Kesselmeier, personal communication, 2013). Thus, the latter reactions could be considered of minor importance, whereas information on peroxy radicals was unfortunately not available.

4.3 Influence of meteorology and air pollution on vertical Damköhler number profiles

The summarized daytime $DA(L_{1-3})$ in Fig. 6c exhibited a pattern of decreasing DA values with layer height. Thus, the likelihood of chemical flux divergence was indicated to decrease from L_1 to L_3. Throughout L_1 to L_3, the τ_{ch} values (Fig. 6a) showed a lower variation compared to the corresponding τ_{tr} (Fig. 6b). Therefore, the daytime DA profile was mainly caused by the vertical τ_{tr} profile.

Interestingly, the nighttime DA of all and the high NO_x periods data showed opposite vertical profiles, indicating an increasing likelihood of chemical flux divergence with increasing layer height (L_1 to L_3). This was especially pronounced during nighttime of the high NO_x periods, where the only instance without indication for a flux divergence within the entire data set was found for L_1. The reasons for this were (i) the extraordinary high $\tau_{ch}(L_1)$ (Fig. 6a and Sect. 4.2), and (ii) the reversed vertical transport time profiles during nighttime (fastest in L_1) of the high NO_x periods (Fig. 6b). This finding agrees very well with Rummel (2005) who found at nighttime the transport timescale in the lowest layer of an Amazonian rainforest to be faster than the chemical timescale.

Above the canopy, the order of magnitude (Fig. 6c) and the median diurnal course (Fig. 3c) of DA compared well with the values of Stella et al. (2013). But the in-canopy DA of Stella et al. (2013) was smaller than the DA above the canopy throughout the entire day, which is in contrast to our study. Considering the canopy flushing time given in Plake and Trebs (2013) (cf. Sect. 4.1.2) and the $\tau_{ch}(L_2)$ (cf. Fig. 6a), a comparable in-canopy DA in Mainz-Finthen was in the order of 2 and 1 for daytime and nighttime, respectively. Thus, in-canopy DA in our study are significantly higher than above the canopy throughout the day. As the canopy height in Stella et al. (2013) was only around 0.2 m, the corresponding transport time was faster with 80 s at noon which could explain

BGD
11, 10737–10777, 2014

the lower in-canopy DA compared to our study. Finally it should be noted that, DA values within plant canopies are not fully representative for all processes, since besides transport and chemistry, additional sources and sinks for trace gases exist within plant canopies. These are specific for each trace gas and will be further discussed below.

4.4 Implications for measured fluxes

4.4.1 Potential NO_x canopy reduction

Within the canopy, $DA(L_{1-2})$ (Figs. 3f, i and 6c) suggested that chemical reactions exhibited a larger influence on the NO-NO_2-O_3 triad during daytime than during night. However, reactive traces gases in canopies are deposited to soil and vegetation elements. Trace gases can be efficiently taken up by plants due to adsorption/absorption on cuticles and diffusion through stomata (e.g., Breuninger et al., 2012). On the other hand, particularly NO is simultaneously produced by microbial processes and is subsequently released from soil. Although, the latter process could be neglected in this study due to insignificant NO soil emissions (Sect. 4.2), the uptake of NO_2 by plants, however, was investigated in order to draw general conclusions on NO_x canopy reduction within natural grasslands canopies. Hence, additional information on the characteristic time scale of plant uptake (τ_u) of NO_2 was required. Such timescales $\tau_u(NO_2)$ integrated over the whole canopy (L_{1+2}) were estimated based on a resistance model (Baldocchi, 1988), following an approach of Rummel (2005) as:

$$\tau_u(x) = \left(\frac{1}{R_{L_x}} \times \frac{\Delta \mathrm{LAI}}{\Delta z} \right)^{-1} \quad (7)$$

BGD
11, 10737–10777, 2014

where x denoted the trace gas of interest (here $x = NO_2$) and R_{L_x} was the leaf resistance of x:

$$R_{L_x} = \left(\frac{1}{R_{bl_x} + R_{s_x} + R_{mes_x}} + \frac{2}{R_{bl_x} + R_{cut_x}} \right)^{-1} \quad (8)$$

with R_{bl_x} being the leaf boundary layer resistance of x calculated according to Personne et al. (2009), R_{s_x} the stomatal resistance of x taken from Plake et al. (2014), R_{mes_x} the mesophyll resistance set to 200 s m^{-1} for NO_2 and R_{cut_x} the cuticular resistance set to 9999 s m^{-1} due to the unimportance of cuticular deposition for NO_2 (both values were taken from Stella et al., 2013).

During daytime, $\tau_u(NO_2)$ was typically found to be the shortest amongst all timescales relevant for NO_2 typically ranging between 90 and 160 s between 09:00 and 17:00 CET (Fig. 7). This timescale was closely followed by $\tau_{ch}(L_{1+2})$ exhibiting values between 100 and 200 s in the same time window, but with a shorter lasting minimum. In contrast, the values of $\tau_{tr}(L_{1+2})$, the canopy flushing time, ranged from 250 to 290 s (Fig. 7) during this time. For a similar canopy with significant NO soil emissions, this would imply an efficient in-canopy conversion of NO to NO_2 during daytime, followed by an effective NO_2 plant uptake as the transport was found to be 2–3 times slower. Furthermore, the biomass density within the lowest 0.2 m of the canopy (i) strongly inhibits the transport, especially in L_1 during daytime (Figs. 5 and 6b), and (ii) dampens the photolysis of NO_2 at the soil–canopy interface, the location where NO is usually emitted. This indicates strong NO_x canopy reduction occurring in such grassland ecosystems during daytime, if the precondition of significant NO soil emissions is fulfilled.

However, during nighttime, $\tau_u(NO_2)$ was found to be very large (Fig. 7), hence, the role of turbulence-chemistry interactions ($DA(L_{1-2})$) was dominating over biological uptake processes. In L_1 the transport of soil emitted NO would be slowest under relatively windy nighttime situations (low NO_x periods in Fig. 3 h) due to undeveloped in-canopy convection. Thus, a considerably high mixing ratio of O_3 within the canopy (Fig. 2e)

BGD
11, 10737–10777, 2014

would lead to an efficient formation of NO_2 indicated by $DA(L_{1-2})$ close to unity. The uptake of NO_2 by plants would be insignificant (see above), and only soil deposition would lead to a small NO_2 depletion. Most likely, such nighttime conditions would lead to simultaneous NO_2 and NO canopy emission fluxes.

However, during nights with low ws (high NO_x periods), the temperature inversion constitutes a "canopy lid". Within the canopy (L_{1+2}) the reaction of residual O_3 (cf. Sect. 4.2) and soil emitted NO would compete with the O_3 surface deposition. Subsequently, a mixture of NO and NO_2 would be trapped inside the canopy. Besides some minor in-canopy NO_2 losses (see above), a distinct NO and NO_2 release may occur in the morning hours, which has been observed for forests (cf. Foken et al., 2012; Dorsey et al., 2004; Jacob and Wofsy, 1990).

4.4.2 Influence on O_3 deposition flux

Similar to NO_2, the application of in-canopy DA values for O_3 remains difficult, since plant uptake and deposition to plant surfaces and the soil are additional O_3 pathways besides chemistry. The characteristic timescale of O_3 plant uptake and soil deposition $\tau_u(O_3)$, shown in Fig. 7, was estimated using Eqs. (7) and (8), with $x = O_3$, R_{mes_x} set to $0\,s\,m^{-1}$ (Erisman et al., 1994) and $R_{cut_x} = R_{ns_x} - R_{soil_x}$ (e.g., Lamaud et al., 2009). R_{ns_x} was taken from Plake et al. (2014) and $R_{soil_x} = 240\,s\,m^{-1}$ according to Lamaud et al. (2009). $\tau_u(O_3)$ ranged from 30 to 150 s, which clearly illustrates the dominance of in-canopy O_3 plant uptake and soil deposition. $\tau_u(O_3)$ was significantly faster than both $\tau_{tr}(L_{1-2})$ and $\tau_{ch}(L_{1-2})$ during the entire day (values are given in Sect. 4.4.1).

Consequently, only DA above the canopy, i.e. $DA(L_3)$ in this study, are valid as an indicator for potential O_3 flux divergence. Because the $DA(L_3)$ always exceeded 0.1 (Figs. 3c and 6c), a chemical flux divergence could not be excluded at the Mainz-Finthen site. Furthermore, $DA > 1$ (Fig. 3c) during the early evening hours clearly indicated potential flux divergence. In the low NO_x periods, the probability of flux divergence was lowest. The influence of chemistry on O_3 deposition fluxes determined by

BGD
11, 10737–10777, 2014

Plake et al. (2014) at the Mainz-Finthen grassland site will be discussed below. The median O_3 fluxes ranged from about −1.5 to −6 nmol m^2 s^{-1} during night and daytime, respectively.

Due to negligible NO soil emissions, a chemical flux divergence in L_3 resulting from counter-directed fluxes of NO and O_3 was very unlikely. Nevertheless, we used a simplified method proposed by Duyzer et al. (1995) based on Reactions (R1) and (R3) and the law of mass conservation. The flux divergence is approximated by the correction factor α_{O_3} as:

$$\alpha_{O_3} = \frac{\phi_x}{\kappa \times u_*} \times \left[k_1 \times \left(N_{NO} \times F^*_{O_3} + N_{O_3} \times F^*_{NO}\right) - j_{NO_2} \times F^*_{NO_2}\right] \quad (9)$$

where $\phi_x = \phi_{O_3} = \phi_H$ was the stability correction function for heat (Högström, 1988), $F^*_{O_3}$ the measured O_3 flux at z_{ref} determined by the eddy covariance method (cf. Plake et al., 2014) and F^*_{NO} and $F^*_{NO_2}$ the corresponding NO and NO_2 fluxes determined by the dynamic chamber technique (cf. Plake et al., 2014). The estimated O_3 deposition flux at z_3 (F_{z_3}) was then calculated as:

$$F_{z_3} = F_{z_{ref}} + \int_{z_3}^{z_{ref}} \left(\frac{\partial F}{\partial z}\right)_z dz = F^*_{O_3} + \alpha_{O_3} \times z_3 \times \left(1 + \ln \frac{z_{ref}}{z_3}\right) \quad (10)$$

where the term $\int_{z_3}^{z_{ref}} \left(\frac{\partial F}{\partial z}\right)_z dz$ was the integrated flux divergence within L_3. The resulting median O_3 flux divergence was quantified to be less than 1 %, confirming the a priori assumption of irrelevant O_3 flux divergence.

Nevertheless, we examined the influence of the enhanced NO mixing ratios in the morning hours (Sect. 3.2, Fig. 2g and h), accompanied by very low O_3/NO ratios (Fig. 8) on the measured O_3 fluxes. A chemically induced O_3 flux $F_c(O_3)$ due to production

BGD
11, 10737–10777, 2014

$P(O_3)$ or loss $L(O_3)$ of O_3 by Reactions (R1) and (R3) integrated over the air column of L_3 was quantified according to Rummel et al. (2007) as:

$$F_c(O_3) = P(O_3) - L(O_3) = \int_{z_3}^{z_{ref}} \frac{\mu_{NO_2}(z) \times \rho_d(z)}{\tau_{NO_2}(z)} \times dz - \int_{z_3}^{z_{ref}} \frac{\mu_{O_3}(z) \cdot \rho_d(z)}{\tau_{O_3}(z)} \times dz \quad (11)$$

where ρ_d (in mol m^{-3}) was the molar density of dry air. τ_{NO_2} and τ_{O_3} (in s) were the chemical depletion times of NO_2 and O_3, respectively:

$$\tau_{NO_2} = \frac{1}{j_{NO_2}} \quad (12)$$

$$\tau_{O_3} = \frac{1}{k_3 \times N_{NO}} \quad (13)$$

Figure 9a displays the diurnal courses of $P(O_3)$ and $L(O_3)$ exhibiting median values of 0 to 1.9 nmol m^{-2} s^{-1} and 0 to −1.4 nmol m^{-2} s^{-1}, respectively. The maximum median values were related to the enhanced NO_x levels in the morning. The resulting median net $F_c(O_3)$ in Fig. 9b ranged between 0.6 and −0.05 nmol m^{-2} s^{-1}, representing a net O_3 production during daytime and a net loss during nighttime. Repeatedly, the medians of low and high NO_x periods adjoined the interquartile range of the overall data set, showing a variability of one order of magnitude of net $F_c(O_3)$ during daytime. Considering the median values of all data, the measured O_3 deposition flux would change by around +10 % during daytime and −3 % during nighttime. This finding is interesting, as to our knowledge previous studies only reported O_3 losses when dealing with the chemical flux divergence of O_3. The outbalancing of the reactions of O_3 with NO (e.g., Dorsey et al., 2004) or VOCs (e.g., Kurpius and Goldstein, 2003) emitted by soil or plants, respectively, resulted in net O_3 loss. The O_3 production in our study was attributed to a deviation from the NO-NO_2-O_3 photostationary state by a surplus of NO_2, based on NO oxidation by e.g. peroxy radicals or other oxidants. Unfortunately, we were

BGD
11, 10737–10777, 2014

not able to assess the impact of these reactions on the calculated chemical timescales as measurements of peroxy radicals were not available. The NO_2 surplus might have originated from simultaneous emissions of non-methane hydrocarbons, carbon monoxide (CO) and NO from motorways surrounding the site in a distance of some kilometers. It is well known that under daytime conditions peroxy radicals are formed that can oxidize NO without consumption of O_3 resulting in net O_3 production (Seinfeld and Pandis, 2006). Although, this O_3 production might also prevail at other experimental sites, this effect is most likely balanced or even exceeded by the destruction of O_3 due to biogenic soil NO emissions which were negligible at our site (a nutrient poor grassland site).

5 Conclusions

For the first time, we simultaneously measured transport times (aerodynamic resistances), vertical profiles of NO-NO_2-O_3 mixing ratios and micrometeorological quantities within and above a natural grassland canopy. The obtained data were analyzed to gain insights about the potential NO_x canopy reduction in the grassland canopy, and to analyze the effect of chemistry on fluxes of purely depositing compounds, such as O_3. We observed two extreme regimes: (a) the first characterized by high wind speed and low NO_x mixing ratios (low NO_x periods) and (b) the second by low wind speed and high NO_x mixing ratios (high NO_x periods). Our study highlights that (i) as a result of in-canopy convection, nighttime transport in the lowest canopy layer is fastest during highly stable conditions above the canopy related to low wind speed (high NO_x periods).

Interestingly, our results on transport-chemistry interactions within the grassland canopy are partly comparable to those found in the Amazonian rainforest, although the vertical canopy structure differs substantially. Natural grasslands exhibit very high biomass densities in the lowest canopy part. Thus, the aerodynamic resistance in the lowest canopy layer (0.04–0.2 m) was found to be of the same magnitude ($> 900\,s\,m^{-1}$) and to feature the same diurnal pattern (higher during daytime, lower at night) as

BGD
11, 10737–10777, 2014

the aerodynamic resistance in the lowest meter of an Amazonian rain forest. The in-canopy aerodynamic resistance representing the whole grassland canopy was at least 3–4 times higher than in-canopy aerodynamic resistances of forest canopies available from literature. Our results reveal that even if the canopy height of natural grassland canopies is small compared to forests (around 1–10 %), the corresponding canopy flushing times are of the same of the same order of magnitude as those reported for forest canopies (10–400 %). The canopy flushing times exhibited only small daytime/nighttime variability, which is well in accordance with a detailed study on flushing times within an Amazonian rain forest (Simon et al., 2005). The small daytime/nighttime variability is caused by the compensating transport efficiencies in lower and upper canopy layers during daytime and nighttime for both canopy types.

The canopy flushing time of the grassland was found to be ≤ 6 min and the chemical timescale of the NO-NO_2-O_3 triad during daytime ranged between 1–3 min. This has obvious implications e.g., for soil emitted reactive compounds such as NO, implying fast chemical conversion of NO to NO_2 within the grass canopy. During daytime the plant uptake of NO_2 was shown to be 2–3 times faster than the canopy flushing time. Inevitably, this leads to a strong potential NO_x canopy reduction in the presence of biogenic NO soil emissions. Due to the extensive global terrestrial coverage with grassland canopies, this finding is highly relevant for the application of global chemistry and transport models. Our results clearly reveal the daytime NO_x canopy reduction for grassland to be much higher than 64 %. Nevertheless, an improved daily averaged NO_x canopy factor analog to the one in Yienger and Levy (1995) cannot be presented here due to the insignificant NO soil emissions at the experiment site.

We determined a median net chemical O_3 production of 10 % during daytime within the air column between the flux measurement and the canopy, which was due to the absence of biogenic NO soil emission in our study. Hence, in contrast to previous studies our measured O_3 deposition flux by eddy covariance is slightly underestimated. The flux divergence for O_3 was one order of magnitude larger during the high NO_x than during the low NO_x periods. In-canopy Damköhler numbers were shown to be relevant

BGD
11, 10737–10777, 2014

for NO_2 only under nighttime conditions, due to the minor role of NO_2 uptake by plants at this time. Above the canopy Damköhler numbers indicated a potential flux divergence, but did not provide a hint for the observed chemical production of O_3. The only instance without indication for a flux divergence within the entire data set was found during nighttime of the high NO_x periods in the lowest canopy layer.

Acknowledgements. This project was funded by the Max Planck Society. We are grateful to J.-C. Mayer for the installation and the maintenance of meteorological sensors and for supporting the data evaluation. We are indebted to A. Moravek for his support with the eddy covariance measurements and the corresponding data evaluation and the fruitful discussions on many details of this study.

The service charges for this open access publication
have been covered by the Max Planck Society.

References

Atkinson, R. and Arey, J.: Gas-phase tropospheric chemistry of biogenic volatile organic compounds: a review, Atmos. Environ., 37, S197–S219, doi:10.1016/S1352-2310(03)00391-1, 2003.

Atkinson, R., Baulch, D. L., Cox, R. A., Crowley, J. N., Hampson, R. F., Hynes, R. G., Jenkin, M. E., Rossi, M. J., and Troe, J.: Evaluated kinetic and photochemical data for atmospheric chemistry: Volume I – gas phase reactions of O_x, HO_x, NO_x and SO_x species, Atmos. Chem. Phys., 4, 1461–1738, doi:10.5194/acp-4-1461-2004, 2004.

Aylor, D. E., Wang, Y. S., and Miller, D. R.: Intermittent wind close to the ground within a grass canopy, Bound.-Lay. Meteorol., 66, 427–448, 1993.

Bakwin, P. S., Wofsy, S. C., Fan, S. M., Keller, M., Trumbore, S. E., and Dacosta, J. M.: Emission of nitric-oxide (NO) from tropical forest soils and exchange of NO between the forest canopy and atmospheric boundary-layers, J. Geophys. Res.-Atmos., 95, 16755–16764, 1990.

Baldocchi, D.: A multi-layer model for estimating sulfur-dioxide deposition to a deciduous oak forest canopy, Atmos. Environ., 22, 869–884, doi:10.1016/0004-6981(88)90264-8, 1988.

BGD
11, 10737–10777, 2014

Breuninger, C., Oswald, R., Kesselmeier, J., and Meixner, F. X.: The dynamic chamber method: trace gas exchange fluxes (NO, NO_2, O_3) between plants and the atmosphere in the laboratory and in the field, Atmos. Meas. Tech., 5, 955–989, doi:10.5194/amt-5-955-2012, 2012.
Crutzen, P.: Discussion of chemistry of some minor constituents in stratosphere and troposphere, Pure Appl. Geophys., 106, 1385–1399, doi:10.1007/Bf00881092, 1973.
Denmead, O. T., Freney, J. R., and Dunin, F. X.: Gas exchange between plant canopies and the atmosphere: case-studies for ammonia, Atmos. Environ., 42, 3394–3406, doi:10.1016/j.atmosenv.2007.01.038, 2007.
Dorsey, J. R., Duyzer, J. H., Gallagher, M. W., Coe, H., Pilegaard, K., Weststrate, J. H., Jensen, N. O., and Walton, S.: Oxidized nitrogen and ozone interaction with forests, I: Experimental observations and analysis of exchange with Douglas fir, Q. J. Roy. Meteor. Soc., 130, 1941–1955, doi:10.1256/Qj.03.124, 2004.
Dupont, S. and Patton, E. G.: Momentum and scalar transport within a vegetation canopy following atmospheric stability and seasonal canopy changes: the CHATS experiment, Atmos. Chem. Phys., 12, 5913–5935, doi:10.5194/acp-12-5913-2012, 2012.
Duyzer, J. H., Deinum, G., and Baak, J.: The interpretation of measurements of surface exchange of nitrogen-oxides – correction for chemical-reactions, Philos. T. Roy. Soc. A., 351, 231–248, doi:10.1098/rsta.1995.0031, 1995.
Erisman, J. W., Vanpul, A., and Wyers, P.: Parametrization of surface-resistance for the quantification of atmospheric deposition of acidifying pollutants and ozone, Atmos. Environ., 28, 2595–2607, doi:10.1016/1352-2310(94)90433-2, 1994.
Finnigan, J.: Turbulence in plant canopies, Annu. Rev. Fluid Mech., 32, 519–571, doi:10.1146/annurev.fluid.32.1.519, 2000.
Foken, T.: Micrometeorology, Springer, Berlin, Heidelberg, 306 pp., 2008.
Foken, T., Meixner, F. X., Falge, E., Zetzsch, C., Serafimovich, A., Bargsten, A., Behrendt, T., Biermann, T., Breuninger, C., Dix, S., Gerken, T., Hunner, M., Lehmann-Pape, L., Hens, K., Jocher, G., Kesselmeier, J., Lüers, J., Mayer, J.-C., Moravek, A., Plake, D., Riederer, M., Rütz, F., Scheibe, M., Siebicke, L., Sörgel, M., Staudt, K., Trebs, I., Tsokankunku, A., Welling, M., Wolff, V., and Zhu, Z.: Coupling processes and exchange of energy and reactive and non-reactive trace gases at a forest site – results of the EGER experiment, Atmos. Chem. Phys., 12, 1923–1950, doi:10.5194/acp-12-1923-2012, 2012.
Gut, A., Scheibe, M., Rottenberger, S., Rummel, U., Welling, M., Ammann, C., Kirkman, G. A., Kuhn, U., Meixner, F. X., Kesselmeier, J., Lehmann, B. E., Schmidt, W.,

BGD
11, 10737–10777, 2014

Muller, E., and Piedade, M. T. F.: Exchange fluxes of NO_2 and O_3 at soil and leaf surfaces in an Amazonian rain forest, J. Geophys. Res.-Atmos., 107, LBA27-21–LBA27–15, doi:10.1029/2001JD000654, 2002.
Hänsel, H. and Neumann, W.: Physik, Spectrum, Akad. Verl., Heidelberg, Berlin, Oxford, 1995.
Hicks, B. B., Baldocchi, D. D., Meyers, T. P., Hosker, R. P., and Matt, D. R.: A preliminary multiple resistance routine for deriving dry deposition velocities from measured quantities, Water Air Soil Poll., 36, 311–330, doi:10.1007/Bf00229675, 1987.
Högström, U.: Non-dimensional wind and temperature profiles in the atmospheric surface-layer – a re-evaluation, Bound.-Lay. Meteorol., 42, 55–78, doi:10.1007/Bf00119875, 1988.
Holzinger, R., Lee, A., Paw, K. T., and Goldstein, U. A. H.: Observations of oxidation products above a forest imply biogenic emissions of very reactive compounds, Atmos. Chem. Phys., 5, 67–75, doi:10.5194/acp-5-67-2005, 2005.
IPPC: Climate Change 2007: The Physical Science Basis, Contribution of Working Group I to the Fourth Assessment Report of the Intergovernmental Panel on Climate Change, University Press, Cambridge, UK, 2007.
Jacob, D. J. and Wofsy, S. C.: Budgets of reactive nitrogen, hydrocarbons, and ozone over the amazon-forest during the wet season, J. Geophys. Res.-Atmos., 95, 16737–16754, doi:10.1029/Jd095id10p16737, 1990.
Jacobs, A. F. G., Vanboxel, J. H., and Elkilani, R. M. M.: Nighttime free-convection characteristics within a plant canopy, Bound.-Lay. Meteorol., 71, 375–391, 1994.
Jäggi, M., Ammann, C., Neftel, A., and Fuhrer, J.: Environmental control of profiles of ozone concentration in a grassland canopy, Atmos. Environ., 40, 5496–5507, doi:10.1016/j.atmosenv.2006.01.025, 2006.
Kasanko, M., Palmieri, A., and Coyette, C.: Land cover/land use statistics, in: Agriculture and Fishery Statistics, edited by: Coyette, C. and Schenk, H., Eurostat, Luxembourg, 158, 2011.
Kruijt, B., Malhi, Y., Lloyd, J., Norbre, A. D., Miranda, A. C., Pereira, M. G. P., Culf, A., and Grace, J.: Turbulence statistics above and within two Amazon rain forest canopies, Bound.-Lay. Meteorol., 94, 297–331, 2000.
Kurpius, M. R. and Goldstein, A. H.: Gas-phase chemistry dominates O_3 loss to a forest, implying a source of aerosols and hydroxyl radicals to the atmosphere, Geophys. Res. Lett., 30, 1371, doi:10.1029/2002gl016785, 2003.
Lamaud, E., Loubet, B., Irvine, M., Stella, P., Personne, E., and Cellier, P.: Partitioning of ozone deposition over a developed maize crop between stomatal and non-stomatal uptakes, using

BGD
11, 10737–10777, 2014

eddy-covariance flux measurements and modelling, Agr. Forest Meteorol., 149, 1385–1396, doi:10.1016/j.agrformet.2009.03.017, 2009.
Lehmann, B. E., Lehmann, M., Neftel, A., Gut, A., and Tarakanov, S. V.: Radon-220 calibration of near-surface turbulent gas transport, Geophys. Res. Lett., 26, 607–610, 1999.
Lenschow, D. H.: Reactive trace species in the boundary-layer from a micrometeorological perspective, J. Meteorol. Soc. Jpn., 60, 472–480, 1982.
Lerdau, M. T., Munger, L. J., and Jacob, D. J.: Atmospheric chemistry – the NO_2 flux conundrum, Science, 289, 2291, doi:10.1126/science.289.5488.2291, 2000.
Mauder, M. and Foken, T.: Documentation and instruction manual of the eddy-covariance software package TK3, Arbeitsergebnisse Nr. 46, 2011.
Monsi, M. and Saeki, T.: Über den Lichtfaktor in den Pflanzengesellschaften und seine Bedeutung für die Stoffproduktion, Jpn. J. Bot., 14, 22–52, 1953.
Monteith, J. L. and Unsworth, M. H.: Principles of Environmental Physics, 2nd edn., E. Arnold, London, New York, 291 pp., 1990.
Moravek, A., Foken, T., and Trebs, I.: Application of a GC-ECD for measurements of biosphere–atmosphere exchange fluxes of peroxyacetyl nitrate using the relaxed eddy accumulation and gradient method, Atmos. Meas. Tech. Discuss., 7, 1917–1974, doi:10.5194/amtd-7-1917-2014, 2014.
Nemitz, E., Sutton, M. A., Gut, A., San Jose, R., Husted, S., and Schjoerring, J. K.: Sources and sinks of ammonia within an oilseed rape canopy, Agr. Forest Meteorol., 105, 385–404, 2000.
Nemitz, E., Loubet, B., Lehmann, B. E., Cellier, P., Neftel, A., Jones, S. K., Hensen, A., Ihly, B., Tarakanov, S. V., and Sutton, M. A.: Turbulence characteristics in grassland canopies and implications for tracer transport, Biogeosciences, 6, 1519–1537, doi:10.5194/bg-6-1519-2009, 2009.
Personne, E., Loubet, B., Herrmann, B., Mattsson, M., Schjoerring, J. K., Nemitz, E., Sutton, M. A., and Cellier, P.: SURFATM-NH3: a model combining the surface energy balance and bi-directional exchanges of ammonia applied at the field scale, Biogeosciences, 6, 1371–1388, doi:10.5194/bg-6-1371-2009, 2009.
Plake, D. and Trebs, I.: An automated system for selective and continuous measurements of vertical thoron profiles for the determination of transport times near the ground, Atmos. Meas. Tech., 6, 1017–1030, doi:10.5194/amt-6-1017-2013, 2013.

BGD
11, 10737–10777, 2014

Plake, D., Stella, P., Moravek, A., Mayer, J. C., Ammann, C., Held, A., and Trebs, I.: Comparison of ozone deposition measured with the dynamic chamber and the eddy covariance method, Agr. Forest Meteorol., submitted, 2014.
Rinne, J., Markkanen, T., Ruuskanen, T. M., Petäjä, T., Keronen, P., Tang, M.J., Crowley, J. N., Rannik, Ü., and Vesala, T.: Effect of chemical degradation on fluxes of reactive compounds – a study with a stochastic Lagrangian transport model, Atmos. Chem. Phys., 12, 4843–4854, doi:10.5194/acp-12-4843-2012, 2012.
Ripley, E. A. and Redman, R. E.: Grassland, in: Vegetation and the Atmosphere, edited by: Monteith, J. L., Acad. Press, London, 349–398, 1976.
Rummel, U.: Turbulent Exchange of Ozone and Nitrogen Oxides Between an Amazonian Rain Forest and the Atmosphere, Ph.D. thesis, Faculty of Biology, Chemistry and Geosciences, University of Bayreuth, Bayreuth, 246 pp., 2005.
Rummel, U., Ammann, C., Gut, A., Meixner, F. X., and Andreae, M. O.: Eddy covariance measurements of nitric oxide flux within an Amazonian rain forest, J. Geophys. Res.-Atmos., 107, 8050, doi:10.1029/2001jd000520, 2002.
Rummel, U., Ammann, C., Kirkman, G. A., Moura, M. A. L., Foken, T., Andreae, M. O., and Meixner, F. X.: Seasonal variation of ozone deposition to a tropical rain forest in southwest Amazonia, Atmos. Chem. Phys., 7, 5415–5435, doi:10.5194/acp-7-5415-2007, 2007.
Seinfeld, J. H. and Pandis, S. N.: Atmospheric Chemistry and Physics: From Air Pollution to Climate Change, 2nd. edn., Wiley, Hoboken, NJ, 1203 pp., 2006.
Simon, E., Lehmann, B. E., Ammann, C., Ganzeveld, L., Rummel, U., Meixner, F. X., Nobre, A. D., Araujo, A., and Kesselmeier, J.: Lagrangian dispersion of Rn-222, H_2O and CO_2 within Amazonian rain forest, Agr. Forest Meteorol., 132, 286–304, 2005.
Stella, P., Kortner, M., Ammann, C., Foken, T., Meixner, F. X., and Trebs, I.: Measurements of nitrogen oxides and ozone fluxes by eddy covariance at a meadow: evidence for an internal leaf resistance to NO_2, Biogeosciences, 10, 5997–6017, doi:10.5194/bg-10-5997-2013, 2013.
Suttie, J. M., Reynolds, S. G., and Batello, C.: Introduction, in: Grasslands of the World, edited by: Suttie, J. M., Reynolds, S. G., and Batello, C., FAO, Rome, 1–17, 2005.
Swinbank, W. C.: A comparison between predictions of dimensional analysis for constant-flux layer and observations in unstable conditions, Q. J. Roy. Meteor. Soc., 94, 460–467, doi:10.1002/qj.49709440203, 1968.

BGD
11, 10737–10777, 2014

Trebs, I., Bohn, B., Ammann, C., Rummel, U., Blumthaler, M., Königstedt, R., Meixner, F. X., Fan, S., and Andreae, M. O.: Relationship between the NO_2 photolysis frequency and the solar global irradiance, Atmos. Meas. Tech., 2, 725–739, doi:10.5194/amt-2-725-2009, 2009.

Trumbore, S. E., Keller, M., Wofsy, S. C., and Dacosta, J. M.: Measurements of soil and canopy exchange-rates in the Amazon rain-forest using Rn-222, J. Geophys. Res.-Atmos., 95, 16865–16873, 1990.

van Pul, W. A. J. and Jacobs, A. F. G.: The conductance of a maize crop and the underlying soil to ozone under various environmental-conditions, Bound.-Lay. Meteorol., 69, 83–99, 1994.

Warneck, P.: Chemistry of the Natural Atmosphere, 2nd edn., Academic Press, San Diego, California, 927 pp., 2000.

Yienger, J. J. and Levy, H.: Empirical-model of global soil-biogenic NO_x emissions, J. Geophys. Res.-Atmos., 100, 11447–11464, doi:10.1029/95jd00370, 1995.

BGD
11, 10737–10777, 2014

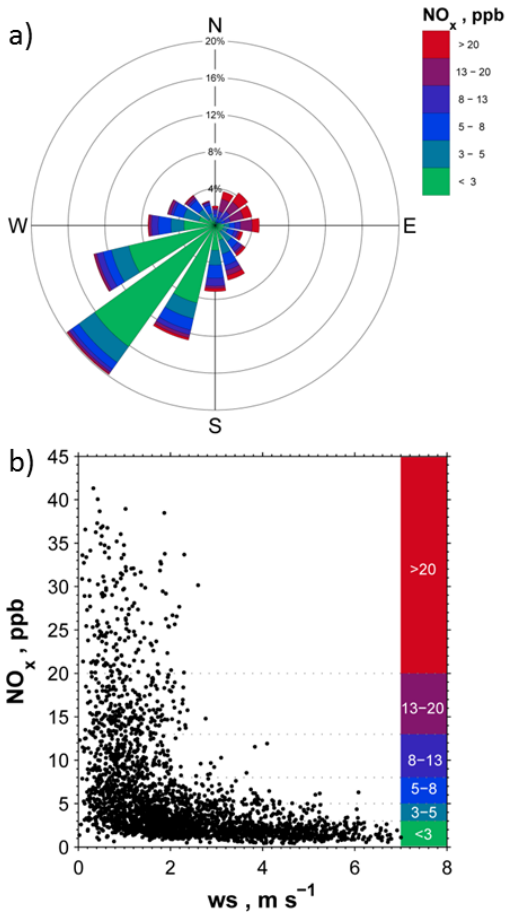

Figure 1. (a) Frequency distribution of wind direction related to NO_x mixing ratios; **(b)** NO_x mixing ratios as function of ws at the Mainz-Finthen grassland site.

BGD
11, 10737–10777, 2014

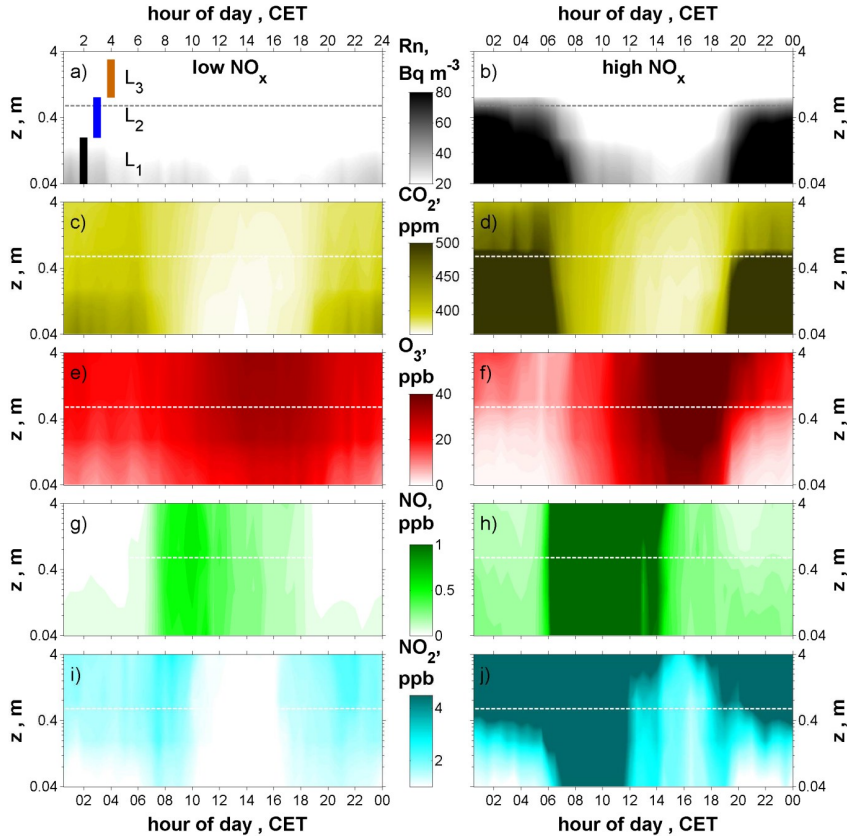

Figure 2. Time height cross sections indicating the median vertical distribution of **(a, b)** Rn, **(c, d)** CO_2, **(e, f)** O_3, **(g, h)** NO and **(i, j)** NO_2 during low NO_x (left panels) and high NO_x (right panels) conditions at the Mainz-Finthen grassland site. The canopy height (dotted line) and L_{1-3} are also shown. The plots were made using the *contourf* function of MATLAB.

BGD
11, 10737–10777, 2014

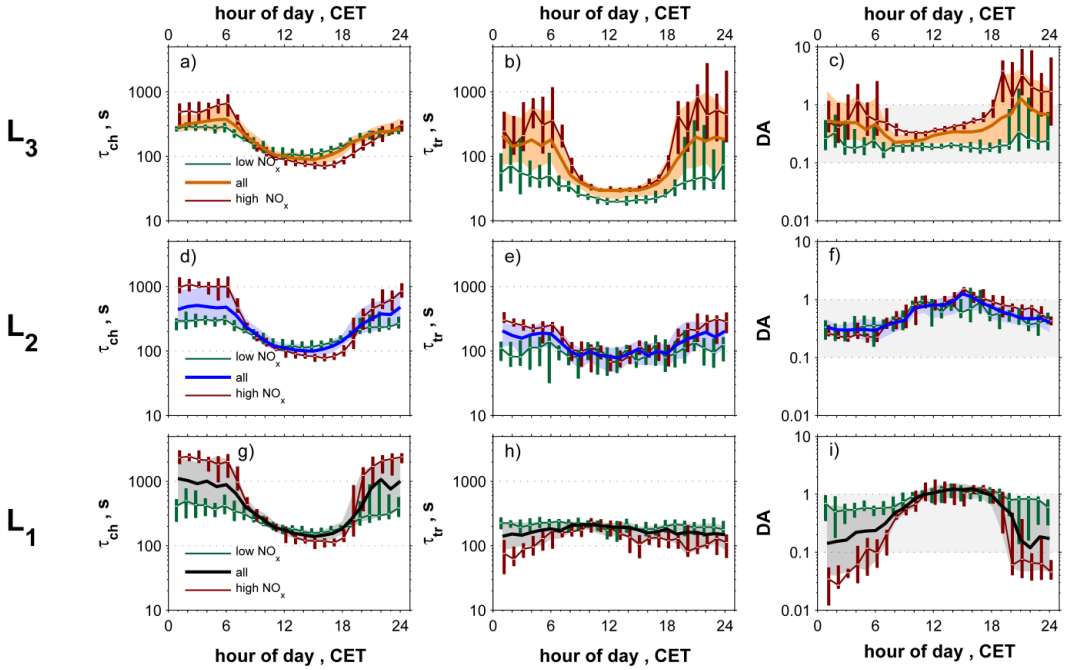

Figure 3. Diurnal courses of **(a, d, g)** $\tau_{ch}(L_{1-3})$, **(b, e, h)** $\tau_{tr}(L_{1-3})$ and **(c, f, i)** $DA(L_{1-3})$ considering all data from 19 August to 26 September 2011 (medians and shaded interquartile ranges) and the low NO_x and high NO_x periods (green and brown medians and interquartile boxes) at the Mainz-Finthen grassland site.

BGD
11, 10737–10777, 2014

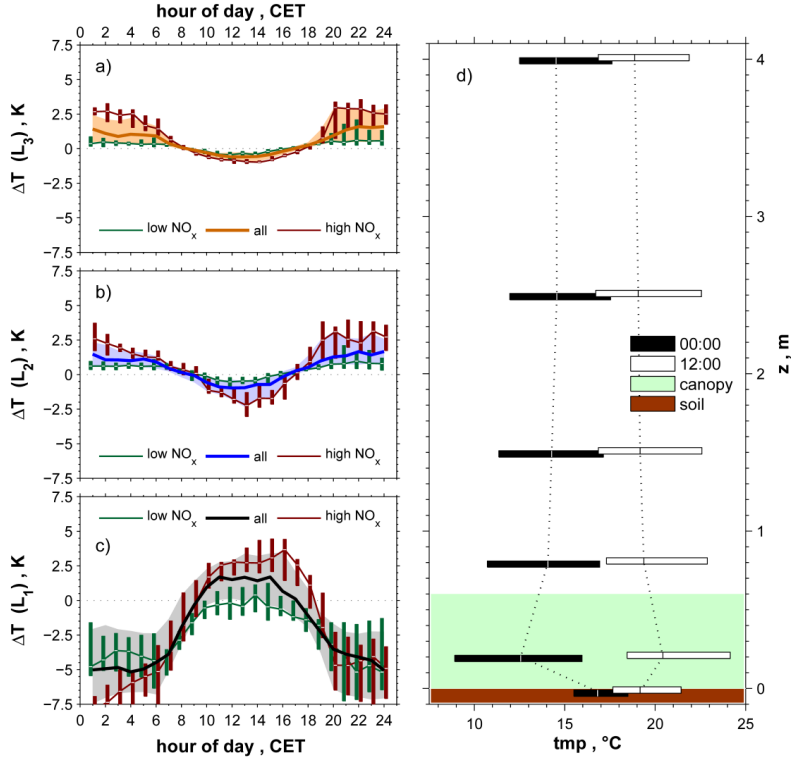

Figure 4. (a–c) Diurnal courses of measured $\Delta T(L_{1-3})$ considering all data from 19 August to 26 September 2011 (medians and shaded interquartile ranges) and the low and high NO_x periods (green and brown medians and interquartile ranges); note: $\Delta T(L_1, L_3)$ do not fully cover L_1 and L_3 (Sect. 2.3) due to availability of measurements (Sect. 2.2); **(a)** $\Delta T(L_3)$: 2.5–0.8 m; **(b)** $\Delta T(L_2)$: 0.8–0.2 m; **(c)** $\Delta T(L_1)$: 0.2–−0.02 m (soil temperature). **(d)** Median vertical temperature profiles and interquartile boxes representing the thermal stratification at 00:00 and 12:00 CET considering all data from 19 August to 26 September 2011 at the Mainz-Finthen grassland site.

BGD
11, 10737–10777, 2014

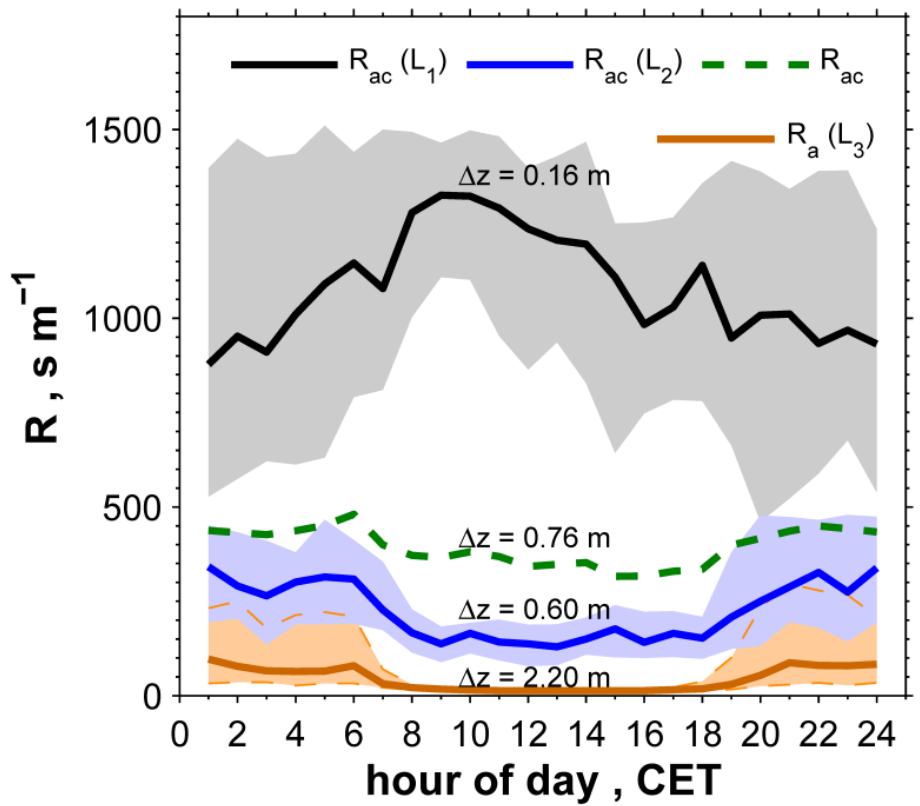

Figure 5. Diurnal courses of in-canopy aerodynamic resistances for each individual canopy layer ($R_{ac}(L_1)$, $R_{ac}(L_2)$) and for the entire grassland canopy (R_{ac}) at the Mainz-Finthen site (median and shaded interquartile ranges). For comparison, the aerodynamic resistance above the canopy is also displayed ($R_a(L_3)$). The layer thickness (Δz) is indicated. The plots includes all data from 19 August until 26 September 2011.

BGD
11, 10737–10777, 2014

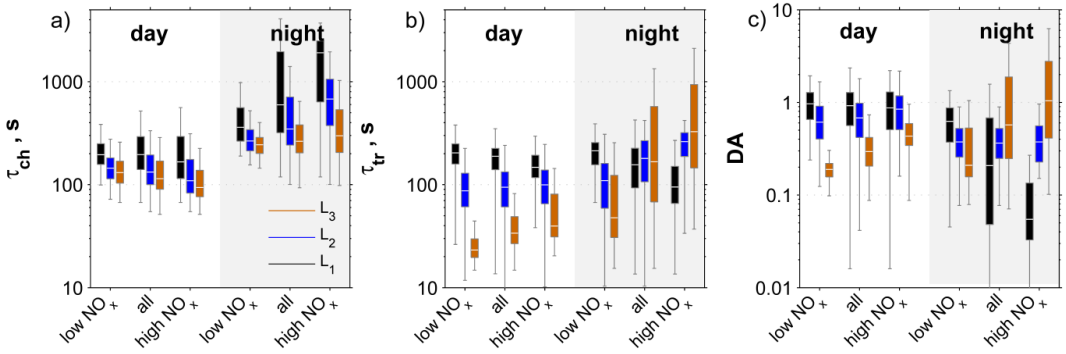

Figure 6. Comparison of box plot statistics for $\tau_{ch}(L_{1-3})$, $\tau_{tr}(L_{1-3})$ and $DA(L_{1-3})$ during daytime and nighttime including all data from 19 August until 26 September 2011 separated for the low and high NO_x periods at the Mainz-Finthen grassland site.

BGD
11, 10737–10777, 2014

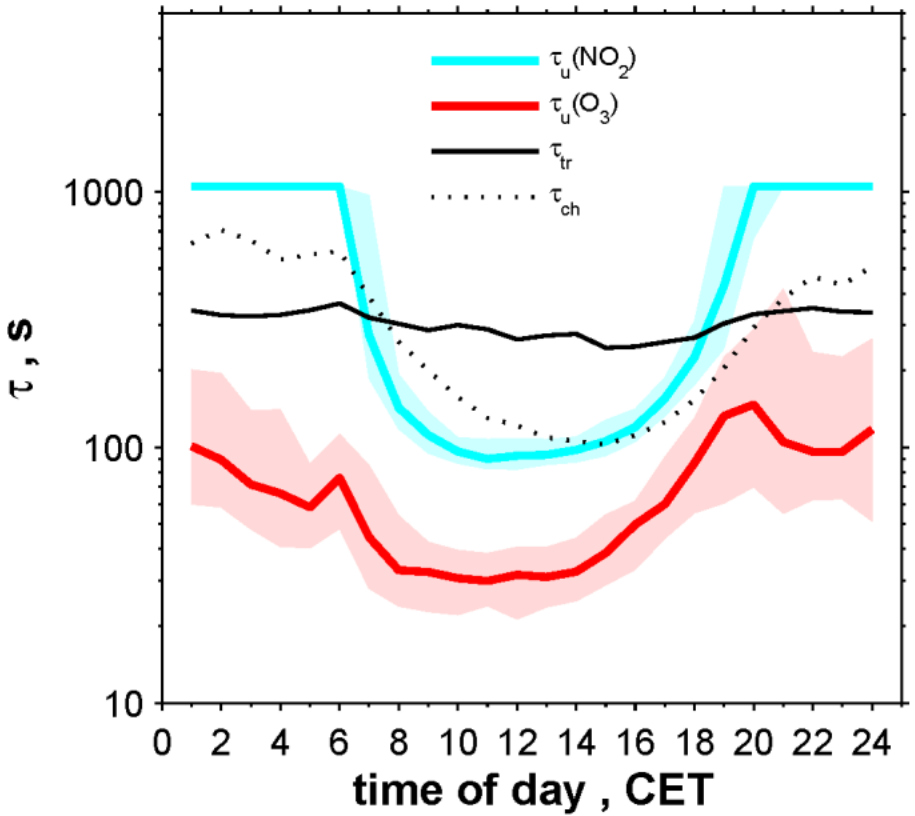

Figure 7. Comparison of median diurnal $\tau_u(NO_2)$, $\tau_u(O_3)$, τ_{tr} and τ_{ch} with interquartile ranges for the whole canopy layer (L_{1+2}) considering all data from 19 August to 26 September 2011 at the Mainz-Finthen grassland site.

BGD
11, 10737–10777, 2014

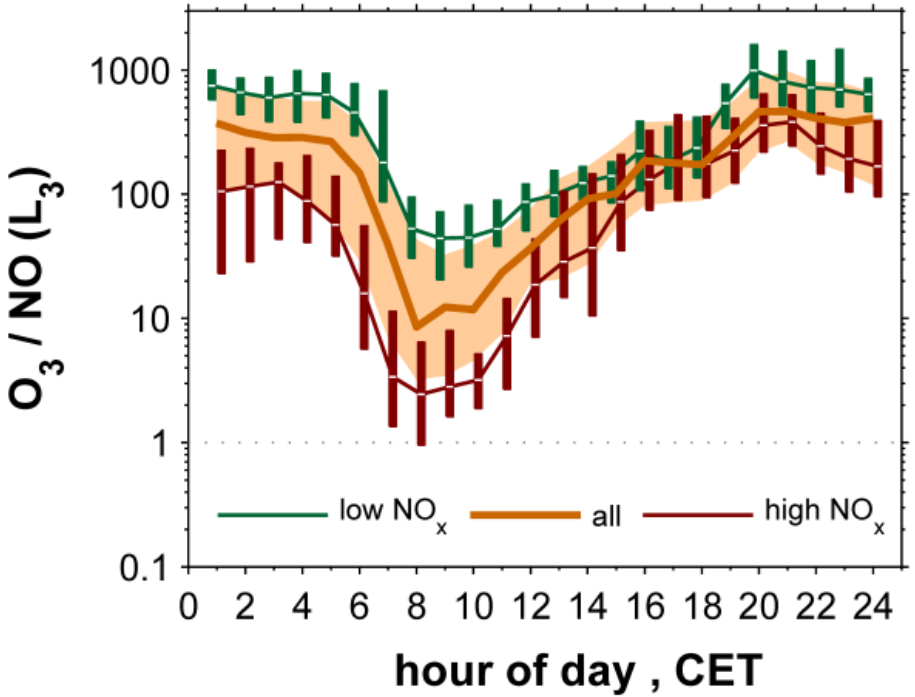

Figure 8. Diurnal course of the O_3 to NO ratio in L_3 considering all data from 19 August to 26 September 2011 (median and shaded interquartile range) and separated for the low NO_x and high NO_x periods (medians and interquartile boxes) at the Mainz-Finthen grassland site.

BGD
11, 10737–10777, 2014

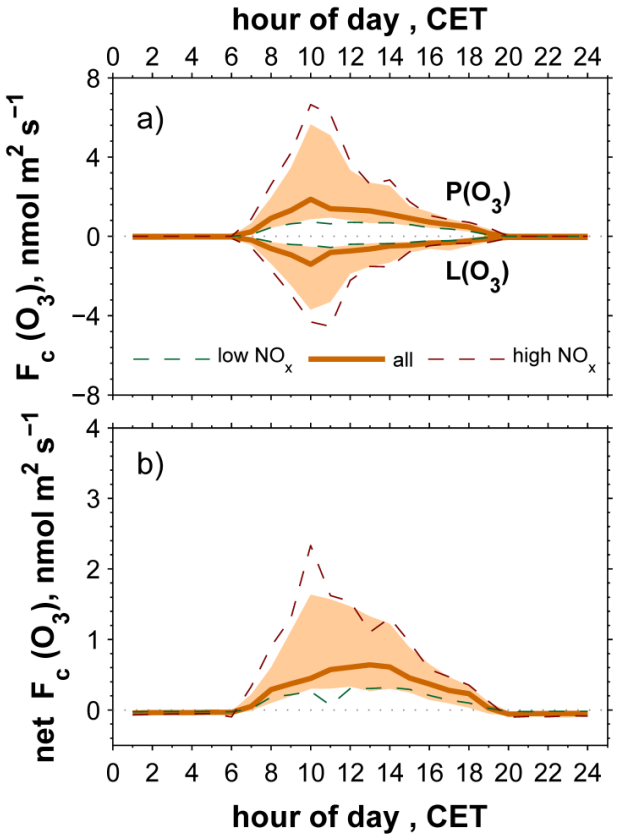

Figure 9. Diurnal courses showing **(a)** $P(O_3)$ and $L(O_3)$ and **(b)** $F_c(O_3)$ (Eq. 11) for L_3 considering all days from 19 August to 26 September 2011 (medians and shaded interquartile ranges) and separated for the low and high NO_x periods (medians) at the Mainz-Finthen grassland site.

BGD
11, 10737–10777, 2014